Draft version April 26, 2024
Preprint typeset using LaTeX style emulateapj v. 04/03/99

MILLIMETRIC GROUND BASED OBSERVATION OF CMBR ANISOTROPY AT $\delta = +28^o$

G. Romeo[1],S. Ali[1], B. Femenía,[2] M. Limon,[3]
L. Piccirillo[1,4,5], R. Rebolo[2], R. Schaefer[6]

Draft version April 26, 2024

ABSTRACT

Results from the third campaign of a ground-based multi-band observation of the millimeter emission of the sky from Tenerife (Canary Islands) are presented. The instrument consists of a 0.45 meter diameter off-axis telescope equipped with a 4-band multi-mode ^3He cooled photometer working at 1.1, 1.3, 2.1 and 3.1 mm wavelengths. The beam is well approximated by a Gaussian with $1^o.35$ Full Width Half Maximum (FWHM) at all wavelengths. The wide wavelength coverage of our instrument allows us to characterize and reduce both the atmospheric and galactic contamination in our data. The CMBR data is analyzed in 6 multipole bands whose centers span the range $\ell = 39$ to $\ell = 134$ at the two longest wavelengths (2.1 and 3.1 mm). A likelihood analysis indicates that we have detected fluctuations in all bands at the two wavelengths. We have evidence of a rise in the angular power spectrum from low ℓ to high ℓ. Our measured spectrum is consistent with current popular theories of large scale structure formation, COBE, and other recent balloon-borne experiments with similar wavelength coverage.

Subject headings: cosmic microwave background — cosmology: observations

1. INTRODUCTION

Precise measurements of the angular power spectrum of the Cosmic Microwave Background Radiation (CMBR) provide strong constraints on cosmological parameters. After the era of the discovery of the anisotropy by COBE (Smoot et al. (1992) and Bennett et al. (1996)) we are now in the age of spatial spectroscopy of the primordial fluctuations. Many experiments have reported detections of anisotropy at different angular scales with evidence of excess of power at angular scales of about $\ell \sim 200$.

We designed an experiment sensitive to a broad angular range ($\ell = 39$ to 134). Our lowest ℓ-band 39^{+38}_{-24} partially overlaps with COBE's highest ℓ-band. The angular range also overlaps with COBE at our longest wavelength (3.1 mm). The partial overlap of the parameters of our experiment and COBE allows us to perform independent consistency checks.

In this letter, we present the data from our third observing campaign of mm-wave CMBR anisotropy from Tenerife (Canary Islands). The first campaign in 1993 was intended to test the instrumental set-up as well as characterize the site. The second campaign in 1994 (see Piccirillo et al. (1997) and Femenía et al. (1998)) measured the anisotropy at two ℓ bands. In the third campaign we extended the angular scale coverage from 2 to 6 bands. Observations were carried out from May to July, 1996.

2. INSTRUMENT

The 1996 Tenerife measurements were performed with the same basic telescope of the 1994 campaign. However, the beam size has been reduced to $1^o.35$ Full Width Half Maximum (FWHM). For details on the instrument see (Femenía (1998)) (Nicholas (1996)), (Ali et al. (2000)), and (Romeo (2000)). Here we briefly summarize its main characteristics. The sky radiation is collected by the primary mirror (0.45 meter diameter). The primary is sinusoidally chopped at 2 Hz with a peak-to-peak amplitude of $5^o.7$ in the sky. The collected radiation is then focused into the photometer by means of a fixed off-axis secondary mirror (0.28 meter diameter). The photometer consists of a 4-band He-3 bolometric system operating at 1.1, 1.3, 2.1 and 3.1 mm wavelengths. The voltage signal from each bolometer is sampled synchronously with the sinusoidal motion of the primary mirror. The sampling rate is 128 samples/channel/second corresponding to 64 samples/channel per sinusoidal cycle of the mirror. In order to minimize systematic effects we surrounded the optics with two levels of radiation shields.

3. CALIBRATION

The primary calibration of the instrument was performed by observing the mm-wave emission of the Moon. Several raster scans of the Moon have been used together with a computer simulation to fit the following parameters: beam size ($1^o.35$), beam throw ($5^o.7$), the calibration constants in Volts/Kelvin for each instrumental band and each demodulation, the azimuth and elevation tracking and pointing accuracy. A model for the Moon emission temperatures was provided by (Gulkis (1998)). A correction for atmospheric attenuation in our bands was estimated from skydips as well as from atmospheric models. The dominant calibration uncertainty comes from the er-

[1]Bartol Research Institute, University of Delaware, Newark, DE, 19716
[2]Instituto de Astrofísica de Canarias, 38200 La Laguna, Spain
[3]Princeton University, Physics Department, Jadwin Hall, Princeton, NJ 08544
[4]University of Wisconsin, Madison, WI, 53706
[5]current address: Department of Physics and Astronomy, Cardiff University, Cardiff CF24 3YB, UK
[6]Raytheon ITSS, NASA Code 664, Goddard Sp. Fl. Ctr., Greenbelt, MD 20771

ror in the Moon temperatures (±5%) and the atmospheric attenuation (±5%). We add these two errors linearly to yield a total calibration uncertainty of ±10%.

4. OBSERVATIONS

Two different observing strategies have been used: the "Dec40" and the "zenith" modes. The Dec40 mode consists of observations in drift scan at a fixed elevation corresponding to $\delta = 40^o$. This declination has been extensively studied at lower frequencies by the Tenerife collaboration (see Gutiérrez et al (1999)) as well as from our instrument in 1994. For the results of our 1996 campaign at declination 40^o see the companion paper (Ali et al. (2000)). The data discussed in this Letter are collected during the "zenith" mode:the telescope is fixed to observe the zenith and the sinusoidal chopping throws the beam along the North-South direction. The East-West sky rotation provides the sampling of a strip of the sky defined by $0h < RA \leq 24h$. This observing strategy is similar to the Saskatoon experiment (see Netterfield et al. (1997)), although we observe at a different declination.

Data were collected from May through June 1996 when atmospheric fluctuations are at their minimum. Any further contamination was minimized by using only the data collected at night, when the Sun was well below the horizon. About 241 hours of data (from 23 nights of observation), corresponding to about 1000 square degrees of sky observed at 4 different wavelengths were collected by using the zenith-mode.

Our zenith observing strategy has the advantage that the telescope does not move during the CMBR observations. This virtually eliminates any changes in the sidelobe pick-up that can contaminate the data due to the motion of the telescope.

5. DATA REDUCTION AND ANALYSIS

Data are demodulated using the following set of orthogonal functions

$$L_n(\omega t) = \cos(n\omega t) + i \sin(n\omega t) = e^{(in\omega t)} \quad (1)$$

where ω is the chopping frequency. The output of the $n-th$ synthesized beam is:

$$a_n + ib_n = \frac{1}{2\pi}\sum_{k=1}^{N} L_n\left(\frac{2\pi k}{N}\right) S_k \quad (2)$$

where S_k are the discrete samples of the bolometer voltages, N=64 is the number of samples per sinusoidal cycle and n=1...6 are the 6 demodulation vectors indices, which can be used to reconstruct a 2-dimensional map of anisotropy (Romeo et al. (2000)). Our choice of orthogonal functions allows us to express the demodulated output according to:

$$\begin{aligned} a_n &= \frac{1}{2\pi}\sum_{k=1}^{N} S_k \cos\left(\frac{2\pi nk}{N} + \psi_n\right) \\ b_n &= \frac{1}{2\pi}\sum_{k=1}^{N} S_k \sin\left(\frac{2\pi nk}{N} + \psi_n\right) \end{aligned} \quad (3)$$

where the $\psi_n = \tan^{-1}(b_n/a_n)$ are phases which account for the instrumental delays between the time ordered data S_k and the position of the beam in the sky. Observations of the Moon signal determine these phases with high accuracy. Each night of observation produces 6 demodulated files per bolometric channel.

The first step in our analysis is to subtract the atmospheric noise from channels 1, 2, and 3 using the information in channel 4, which is the most sensitive to atmospheric noise. Our technique is essentially the same as used in the analysis of our 1994 campaign data (Nicholas (1996), Femenía et al. (1998), and Piccirillo et al. (1997)) which was already an improved version of the technique used by Andreani et al. (1991). The details of the procedure are to be found in Romeo (2000) and Ali et al. (2000). A more general theoretical discussion can be found in Melchiorri et al. (1996). The atmospheric subtraction can only be applied when the atmospheric conditions are stable and there is a strong correlation (> 75%) between channel 4 and the other channels. In the lower harmonics, the power spectra of the atmospheric subtracted data show a strong improvement in the signal to noise ratio. For the higher harmonics (n = 4, 5, and 6), we did not need the atmospheric subtraction because the high degree of spatial differencing breaks up the atmospheric noise, whose power decreases sharply with scale. (Atmospheric noise follows a Kolmogorov power spectrum which decreases as the wavenumber to the -8/3 power.) A more in-depth analysis of the atmospheric noise will be discussed in even greater detail in Ali (2000) and Ali et al. (2000).

Long term drifts in the data are then removed by fitting a combination of sine and cosine functions(Femenía et al. (1998) and Femenía (1998)). The spatial frequencies used correspond to angles of 90, 60, 30, 30, 30 30 degrees R. A. for demodulations 1-6 respectively, angular scales where the window functions are negligible. Data are finally stacked together and binned in RA intervals of about $1^o.4$.

The final data set is analyzed by performing a likelihood analysis of each individual demodulation for the two longest wavelength bands (3.1 and 2.1 mm) corresponding to 6 ℓ ranges centered from ℓ=39 to ℓ=134. In fig. 1 we show the first demodulation of the bands together with the demodulations obtained by simulating our observing strategy on the DIRBE 240 μm map . The feature visible in the DIRBE demodulations at RA about 20h is the region corresponding to the crossing of the galactic plane. We see that the same feature is visible in the 1.3 mm band and somewhat less visible with increasing wavelength to 2.1 and 3.1 mm.

We can use the ratios of intensities I(DIRBE)/I(mm) to extrapolate the galactic signal in the region of $12 < RA < 19$ where we analyze the data for CMBR anisotropy. The result of the extrapolation is shown in fig. 2. We see that, at high galactic latitude, in the two longest wavelength bands (1 and 2) the galactic contamination should be negligible while the band at 1.3 mm might be contaminated by residual galactic dust emission and is not included in this analysis.

Computing the various window functions is the last step needed to perform the likelihood analysis. The relative simplicity in the observing strategy comes at the cost of some algebra in computing the window functions for each individual demodulation at any angular lag. Following

(White and Srednicki (1994)), the expression for the window function of each demodulation is:

$$W_\ell^n(\hat{k}_i \cdot \hat{k}_j) = \aleph^2 B_l^2 \Bigg\{ \left[Q_{\ell,0}^n(\theta_o) \right]^2 + 2 \sum_{m=1}^{\ell} \frac{(\ell-m)!}{(\ell+m)!} \times \cos(m(\phi_i - \phi_j)) \left[Q_{\ell,m}^n(\theta_o) \frac{\sin(\frac{m\Delta\phi}{2})}{\frac{m\Delta\phi}{2}} \right]^2 \Bigg\} \quad (4)$$

where n is the integer for the corresponding demodulation, $\hat{k}_i$ and $\hat{k}_j$ are respectively the unit vectors identifying right ascension bin i and j, $\aleph$ is the normalization determined in the same way as for Saskatoon [see White and Srednicki (1994)],

$$B_\ell(\sigma) = \exp\left[-\frac{1}{2}\ell(\ell+1)\sigma^2 \right]$$

is the beam profile function with σ=0.^{o}57, our Gaussian beam width, and

$$Q_{\ell,m}^n(\theta_o) = \frac{\omega_c}{2\pi} \int_{-\pi/\omega_c}^{\pi/\omega_c} L_n(t) P_\ell^m[\cos(\theta(t))]dt \qquad \mathrm{m} = 0...\ell$$

where $L_n(t)$ is the lock-in function in equation 1, $P_\ell^m[\cos(\theta(t))]$ is the associated Legendre polynomials, $\Delta\phi$ is the binning size in Right Ascension, and finally $\theta(t) = \theta_o + \alpha \sin(\omega t)$, with $\theta_o = 28^o$, and $\alpha = 2^o.84$.

The window functions are estimated numerically.

6. STATISTICAL ANALYSIS

The statistical analysis used to determine the amplitude of the fluctuation in the CMB was performed by using the Likelihood defined as follows:

$$\mathcal{L} = \frac{1}{(2\pi)^{N/2}|\mathbf{M}|^{1/2}} \exp\left(-\frac{1}{2} t^T \mathbf{M^{-1}} t \right) \quad (5)$$

where t is the vector containing the demodulated and stacked data. We maximize the likelihood L for channels 1 and 2 both individually and collectively. Each channel has 72 1.4 degree bins of stacked data for each harmonic, so the covariance matrix M is a 72 x 72 (144 x 144) matrix for the individual (combined) likelihood, respectively. The combined channel analysis includes terms for the correlation between channels. The covariance matrix is the sum of two matrices, signal (S_{ij}) and noise (N_{ij}). The signal is given by

$$S_{ij} = \frac{1}{4\pi} \sum_{\ell=1}^{\infty} (2\ell+1) C_\ell W_\ell^n(\hat{n}_i \cdot \hat{n}_j)$$

where $W_\ell^n(\hat{n}_1 \cdot \hat{n}_2)$ is the window function, and C_ℓ are the usual temperature angular correlation coefficients. The noise covariance matrix is

$$N_{ij} = \sigma_i \sigma_j C_{ij}$$

where C_{ij} is the correlation function obtained from the data. Because of the symmetry of the covariance matrix we can use Cholesky factorization to invert $\mathbf{M}$. For the signal autocorrelation function, we used a flat spatial temperature fluctuation spectrum parametrized by the quadrupole amplitude ΔT (see e. g., Schaefer and deLaix (1996))

$$C_\ell = \frac{6\sqrt{(\pi)}}{5} (\Delta T)^2 \frac{2\ell+1}{\ell(\ell+1)}. \quad (6)$$

ΔT is then fit to the data and the result is converted to band power. We obtain very consistent results separately for channels 1 and 2 which are shown in table 1 along with the combined channel results. Results for channel 1 and 2 are in Table 1. The reported 68% confidence levels have been calculated in the usual way (see Church et al. (1997)), and do not include calibration uncertainty. In Figure 3, we show two theoretical structure formation models for comparison, the "standard" cold dark model and a spatially flat cosmological constant (Λ) dominated model. We see that our data are consistent with the rise to the "Doppler peak" expected in currently popular adiabatic theories of structure formation (like the models shown.)

The cosmic origin of our signal has been further checked with the following null test: we divided the set of the stacked data files in two subsets; the likelihood analysis of their sum and difference produced respectively results consistent with those in Table 1, and with zero (see Romeo (2000)) .

We can also calculate the overlap window functions between different lock-in patterns and angular lags and use it to estimate the correlations between harmonics, similar to the method in (Netterfield (1995)). The amplitude of the correlated harmonics was calculated using these overlap window functions and a flat CMB spectrum, normalized so the diagonal elements are unity. We found that correlations between signals measured by the various harmonics are for the most part negligible ($<$ 1%). Even-odd pairs of harmonics are completely uncorrelated. There is some non-negligible correlation between pairs of either odd-odd or even-even harmonics. The correlations between harmonic pairs 1-3, 2-4, 3-5, and 4-6 are 0.42, 0.53, 0.61 and 0.67, respectively. We verified that these correlation terms are detectable in a likelihood analysis of the data and are consistent with our estimates. The correlations between pairs 1-5 and 2-6 are much smaller: 0.03 and 0.04, respectively. If one wants to be conservative in using these points to constrain cosmological parameters, one can use one even-odd pair of harmonics and be assured that those two points will be completely independent.

Finally we compare our results with other experiments in Figure 3. We see that our lowest l-band temperature measurement is completely consistent with COBEs highest l-band temperature fluctuation measurement. Furthermore, we plot results from two recent balloon experiments done at similar wavelengths, BOOMERanG (de Bernardis, et al. (2000)), and MAXIMA (Hanany et al. (2000)). (For a more complete summary of experimental results, see Max Tegmark's CMB web site at http://www.sns.ias.edu/max/cmb/experiments.html.) We see that our results are remarkably consistent with those of other experiments, which observed a different part of the sky, and used completely different experimental and analysis techniques.

7. CONCLUSION

Improvements in our instrumental setup over our 1994 campaign, as well as refinements in our data analysis procedure, have allowed us to detect temperature fluctuations over a wide range of angular scales. We have used data from our 4-band detector to reduce the atmospheric noise contamination and to delineate regions of our scans for which the galactic contamination is insignificant. We find positive detections of residual temperature fluctuations in 6 angular ranges in our two longest wavelength bands (2.1 mm and 3.1 mm). These measurements, summarized in table 1, are our main result. The derived temperatures are consistent with those seen in other experiments . Our results essentially show a monotonically increasing amplitude of temperature fluctuation with l, and are consistent with some currently popular adiabatic theories of cosmological structure formation.

This work was supported by a University of Delaware Research Foundation (UDRF) grant, and by the Bartol Research Institute. We also want to thank the technical staff of the Observatorio del Teide, and finally R. Hoyland, B. Watson, L. Shulman and G. Poirer for their help.

REFERENCES

Ali S. 2000, “Measurement of Anisotropy in Cosmic Background Radiation ”, University of Delaware, Doctoral Thesis (Adv. L. Piccirillo)
Ali, S. et al 2000, In preparation
Andreani, P, Dall’Oglio, G., Martinis, L, Piccirillo, L., Pizzo, L., and Rossi, L., 1991 AA 249 299
Bennett, C. L. et al., 1996 ApJ464 L1
Church, S. E.,Ganga, K. M., Ade, P. A. R., Holzapfel, W. L., Mauskopf, P. D., Wilbanks, T. M.; Lange, A. E. 1997 ApJ484 523
de Bernardis, P., et al. 2000 Nature 404 955
Femenía B., Rebolo R., Gutiérrez, C. M., Limon, M., Piccirillo, L. 1998, ApJ, 498, 117
Femenía C. B. 1998, “Millimetric Ground Based Observation of CMB Anisotropy”, Instituto De Astrofísica De Canarias, Doctoral Thesis (Adv. R. Rebolo)
Gulkis S., private communication 1998
Gutiérrez, C. M., Rebolo, R., Watson, R. A., Davies, R. D., Jones, A. W., Lasenby, A. N., Submitted to Apj astro-ph/9903196
Hanany S., et al. 1996, astro-ph/0005123
Melchiorri, B., de Petris, M., D’Andreta, G., Guarini, G., Melchiorri, F., Signore, M., ApJ471, 52
Netterfield, C. B., Devlin, M. J., Jarolik, N., Page, L., Wollack, E. J. 1997, ApJ, 474, 47
Netterfield, C. B.,1995 “A Measurement of the Degree Scale Anisotropy in the Cosmic Microwave Background Radiation”, Princeton University Doctoral Thesis
Nicholas M. J. 1996, “Observations of Cosmic Microwave Background Radiation Anisotropy”, University of Delaware, Doctoral Thesis (Adv. L. Piccirillo)
Page L., 1998, Proceedings from the Third International School of Particle Astrophysics: ”Generation of Large Scale Cosmological Structures,” Erice, Sicily
Piccirillo L. et al., 1997 ApJ, 475, L77
Romeo, G. et al, 2000 In preparation
Romeo G. 2000, “Millimetric Ground-Based Observation of CMBR Anisotropy at Declination $+28^o$”, University of Delaware, Doctoral Thesis (Adv. L. Piccirillo)
Schaefer, R.K and De Laix, A.A., 1996, Ap. J. S., 105, 1
Seljak U. and Zaldarriaga M., 1996 ApJ469 437-444
The CMBFAST code is available at
http://www.sns.ias.edu/∼matiasz/CMBFAST/cmbfast.html
Smoot G. F., et al. 1992 ApJ, 396 L1
Tegmark, M. and Hamilton, A., 1997, Physics Review D, 55, 5895
White, M., and Srednicki, M. 1995, ApJ, 443, 6

Fig. 1.— The first harmonics of thermodynamic temperature differences in the three channels.The thick line is the result of simulating our observing pattern on the DIRBE 240 μ m map of the sky, scaled to the corresponding wavelength. The scaling factors are respectively 5.0, 5.4, and 30.8 μK/MJy/sr for our 3.1 mm, 2.1mm, and 1.3 mm wavelength channels.

Fig. 2.— Comparison between Galactic Dust Emission and CMB anisotropy. The galactic dust emission for each channel has been evaluated in the galactic plane crossing region (RA = 19-21 hours) and extrapolated to the other region (RA = 12 - 19 hours), using information from the first harmonic on real data and the simulated observations on the DIRBE map (see figure 1). This is done for channels 1, 2, and 3. The spectral index of the galactic dust emission is estimated to be $1.5 \pm 1.$ from fitting a power law line to the data shown above.

Fig. 3.— Band power vs. l for all harmonics. We have obtained the theoretical curves using CMBFAST (Seljak and Zaldarriaga (1996)). Shown are "standard CDM" (Ω_{CDM}, Ω_Λ, Ω_b, n, $h = H_0/100\ km\ s^{-1}\ Mpc^{-1}$) = (0.95, 0.00, 0.05, 1.0, 0.65) and Λ CDM (0.35, 0.60, 0.05, 1.0, 0.65). The data shown are from this experiment, COBE (Tegmark and Hamilton (1997)), and two other recent experiments using similar wavelengths - BOOMERanG (de Bernardis, et al. (2000)) and MAXIMA (Hanany et al. (2000)).

Table 1

Summary of Band Powers μK for channel 1 and 2 as determined by the likelihood analysis.

Harmonic	$\bar{\ell}$	Channel 1	Channel 2	Channel 1 + Channel 2
1	39^{+38}_{-24}	33^{+11}_{-9}	35^{+13}_{-9}	34^{+8}_{-6}
2	61^{+28}_{-22}	41^{+12}_{-10}	40^{+9}_{-8}	40^{+7}_{-6}
3	81^{+27}_{-20}	43^{+16}_{-14}	40^{+10}_{-9}	41^{+8}_{-8}
4	99^{+24}_{-18}	48^{+17}_{-15}	51^{+13}_{-11}	50^{+10}_{-9}
5	116^{+23}_{-14}	49^{+18}_{-14}	44^{+13}_{-11}	46^{+10}_{-9}
6	134^{+20}_{-12}	60^{+28}_{-35}	56^{+12}_{-11}	56^{+11}_{-10}

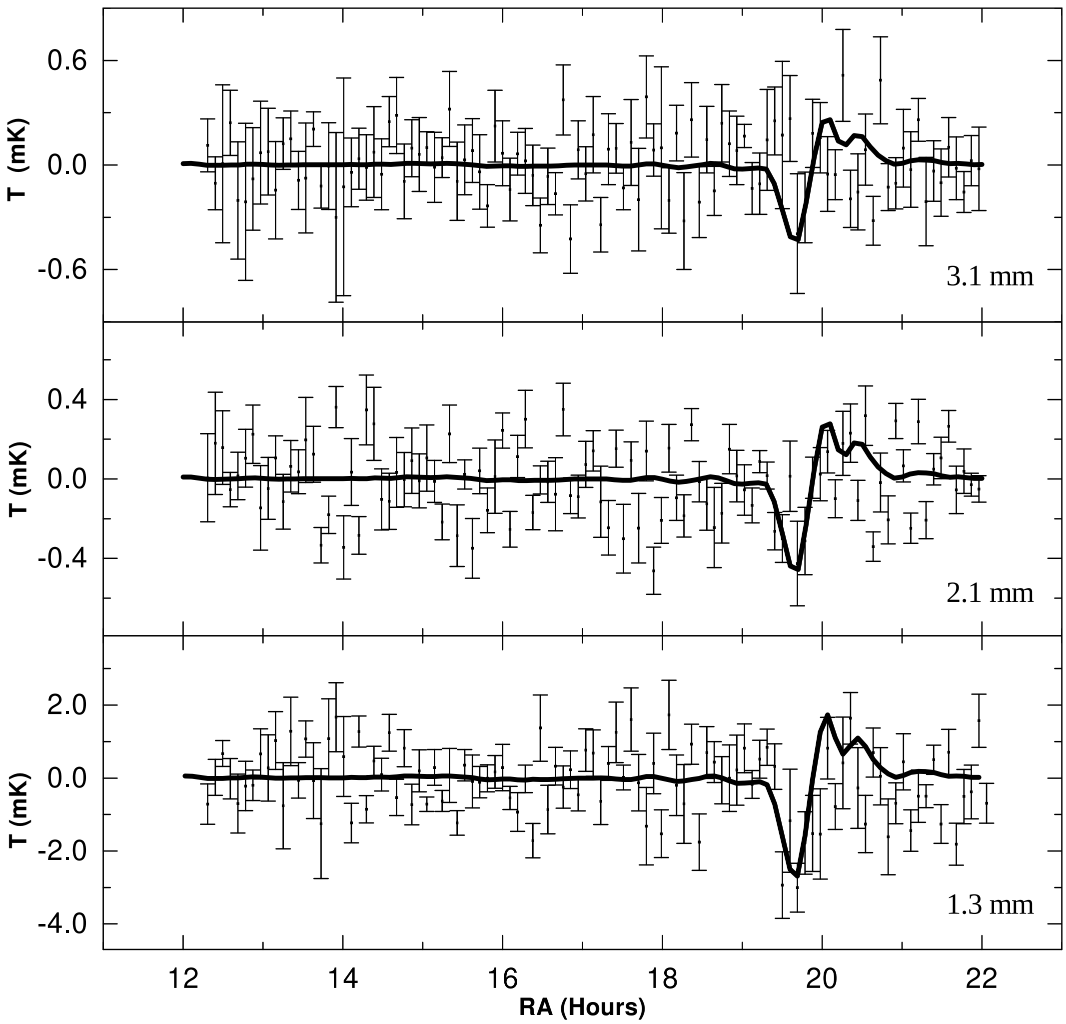
0.6
0.0
-0.6
T (mK)
3.1 mm
0.4
0.0
-0.4
T (mK)
2.1 mm
2.0
0.0
-2.0
-4.0
T (mK)
1.3 mm
12
14
16
18
20
22
RA (Hours)

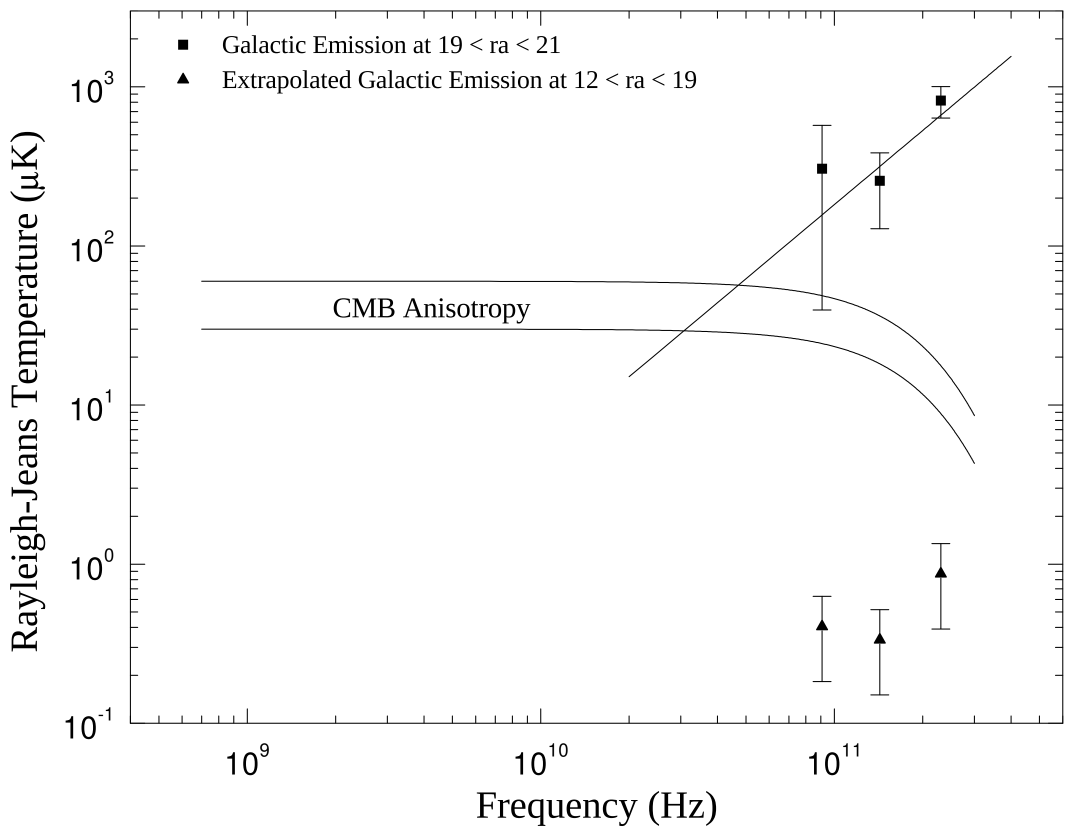
Galactic Emission at 19 < ra < 21
Extrapolated Galactic Emission at 12 < ra < 19
CMB Anisotropy
Rayleigh-Jeans Temperature (μK)
Frequency (Hz)
10^3
10^2
10^1
10^0
10^-1
10^9
10^10
10^11

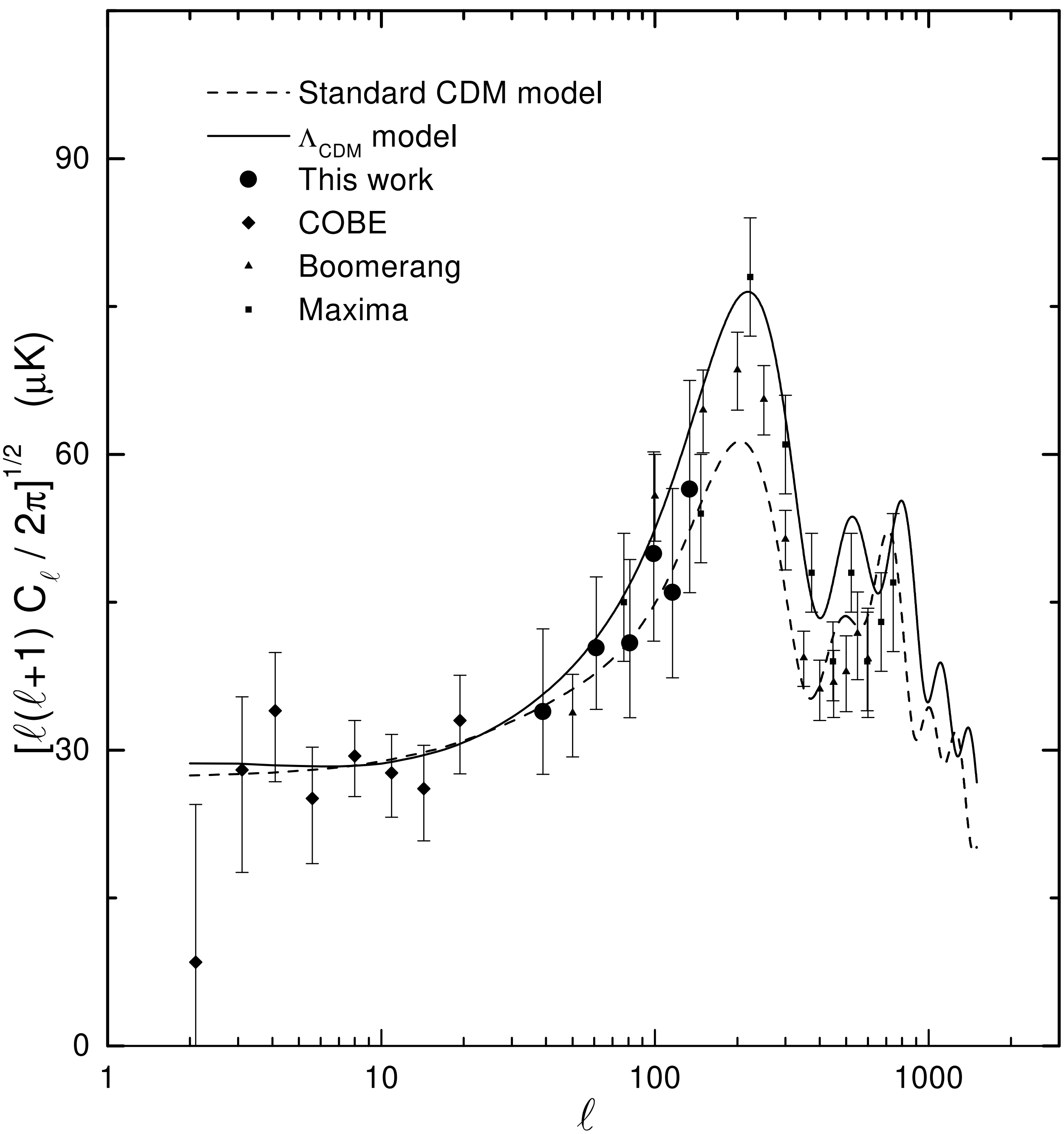
Standard CDM model
Λ_{CDM} model
This work
COBE
Boomerang
Maxima
$[\ell(\ell+1)\ C_\ell\ /\ 2\pi]^{1/2}$ (μK)
90
60
30
0
1
10
100
1000
ℓ